

# Study of transport coefficients in ultrarelativistic kinetic theory

Victor E. Ambruş<sup>1,\*</sup>

<sup>1</sup>*Department of Physics, West University of Timișoara,  
Bd. Vasile Pârvan 4, 300223 Timișoara, Romania*

(Dated: December 14, 2024)

## Abstract

The connection between the relativistic Boltzmann equation and the dissipative hydrodynamics equations is traditionally made through the Chapman-Enskog procedure or through Grad's moment approximation. While the ensuing transport coefficients predicted by the two approaches coincide in the non-relativistic limit, in general their ultra-relativistic limits differ. In this paper, we consider a spatially-periodic longitudinal wave in relativistic dissipative hydrodynamics. At sufficiently small velocities, we obtain an analytic solution in the linearised limit of the macroscopic conservation equations. We then use a kinetic solver to obtain the numerical solution of the relativistic Boltzmann equation for massless particles in the Anderson-Witting approximation for the collision term. We find that the transport coefficients emerging from the relativistic Boltzmann equation agree with those predicted through the Chapman-Enskog procedure.

---

\* E-mail: victor.ambrus@e-uvt.ro

## I. INTRODUCTION

The relativistic Boltzmann equation is known to reduce to the equations of relativistic hydrodynamics in the limit when the mean free path of the particle constituents is negligible compared to the typical length scales of the system [1]. The transition from kinetic theory to relativistic hydrodynamics is traditionally performed following two approaches: the Chapman-Enskog procedure and the moments approximation [1]. These two approaches yield different expressions for the transport coefficients appearing in the constitutive equations of the underlying hydrodynamic equations. While the non-relativistic limit of these expressions coincides between the two formulations, their ultrarelativistic limit differs.

In order to check which one of the two approaches (Chapman-Enskog expansion or the moment approximation) correctly predicts the transport coefficients of the hydrodynamic equations, a solution of the relativistic Boltzmann equation is required. Solving the Boltzmann equation requires an explicit expression for the collision term, which in general is an integral operator taking into account local binary collisions. A considerable simplification arises by employing a single relaxation time (SRT) approximation. The most common SRT approximations are the Marle [2] and the Anderson-Witting [3, 4] models. Since it is known that the Marle model is not appropriate for massless particles [1, 3], we will only consider the Anderson-Witting model in this paper.

There has been recent evidence in the literature indicating that the transport coefficients predicted by the Chapman-Enskog method are closer to those recovered from solutions of the Boltzmann equation than those obtained through the moment approximation.

Florkowski et al. obtained an analytic solution of the Anderson-Witting-Boltzmann (AWB) equation in the case of Bjorken flow [5] at non-vanishing relaxation times, written in integral form for the case when the distribution function depends only on proper time. This solution was restricted to the massless case in Refs. [6, 7] and extended to the massive case in Ref. [8]. In Refs. [6, 7], it is shown that the numerical solution of the Israel-Stewart equations [9] leads to better agreement with the AWB solution (computed also numerically) when the Chapman-Enskog value for the shear viscosity is used compared to when the 14 moment approximation is used. The same conclusion is reached in Ref. [10] for the case of Bose-Einstein and Fermi-Dirac statistics.

The solution of the AWB equation describing the Bjorken flow of massive particles ob-

tained in Ref. [8] is used in Ref. [11] to highlight that the second order Chapman-Enskog expansion is in closest agreement to the solution of the AWB equation as compared to the Israel-Stewart [9] and the 14 moment approaches introduced in Ref. [12].

Bhalerao et al. [13] have demonstrated in the context of heavy-ion collisions that “Grad’s method leads to the violation of the experimentally observed  $1/\sqrt{m_T}$  scaling of the longitudinal femtoscopic radii,” [13] while the Chapman-Enskog method does not exhibit such an unphysical behavior.

The relativistic lattice Boltzmann (LB) method has also been used as a tool to solve the AWB equation [14–23]. The propagation of a shock wave of massless [14, 16–19] and massive [21, 22] particles is investigated using the LB method and the results are validated by comparison with the data obtained using the Boltzmann Approach to Multi Partion Scattering (BAMPS) reported in Refs. [24–26]. In order to compare the LB results obtained in the frame of the AWB equation and the BAMPS results, the shear viscosity to entropy ratio  $\eta/s$  must be kept constant. Matching within the LB method the values of  $\eta/s$  employed in the BAMPS simulations requires as an input the exact expression for the shear viscosity  $\eta$ , which can be obtained via Grad’s 14 moment approach [14, 16–18, 21] or the Chapman-Enskog procedure [19, 22]. The authors of Refs. [19, 22] note that employing the Chapman-Enskog value for  $\eta$  leads to better agreement with the BAMPS data than when the Grad value is employed.

Recently, the relativistic lattice Boltzmann model developed in Ref. [21] was used in Ref. [22] to study the dissipative attenuation of the relativistic equivalent of the Taylor-Green vortices. This study allowed the authors of Ref. [22] to demonstrate that the correct value of the shear viscosity is that given by the Chapman-Enskog procedure rather than the Grad method for a wide range of particle masses.

In this paper, we present a study of the transport coefficients arising in the Anderson-Witting model by considering the dissipative attenuation of a harmonic longitudinal wave. In the regime of small amplitudes, the linearised form of the first order relativistic hydrodynamic equations can be solved analytically (i.e. in the five-field approximation). The wave amplitude predicted by the analytic solution consists of a damped oscillatory term (with respect to time) which allows the wave to propagate at (about) the speed of sound, for which the attenuation coefficient  $\alpha_d$  is directly proportional to the shear viscosity  $\eta$ . The second term is non-oscillatory and its attenuation coefficient  $\alpha_\lambda$  is directly proportional to the

heat conductivity  $\lambda$ . Depending on the initial conditions, this system allows  $\eta$  and  $\lambda$  to be measured separately, providing unambiguous indication that the correct expressions for the transport coefficients in the AWB equation are those obtained through the Chapman-Enskog expansion rather than through the 14 moment approach.

We test the robustness of our proposed setup by considering various values of the wave amplitude and of the relaxation time. According to Refs. [19, 20], high order quadratures (i.e. large velocity sets) are required to obtain accurate simulation results at large values of the relaxation time, when the flow is out of equilibrium and rarefaction effects become important. We thus perform our numerical experiments using the R-SLB models developed in Ref. [19], since these models are easily extendable to arbitrarily high quadrature orders. While the analysis presented in this paper is restricted to the case of massless particles, it can be easily extended to the case of massive particles, e.g. following Refs. [21, 22, 27].

The paper is organised as follows. In Sec. II, we briefly review the basics of the Boltzmann equation in the Anderson-Witting single-time approximation (the AWB equation) and introduce our notation. In Sec. III, we derive the relativistic hydrodynamics equations linearised with respect to small perturbations. In Sec. IV, we derive an analytic solution of these equations within the five-field theory for the dissipative attenuation of a longitudinal wave. In Sec. V, we employ the R-SLB models introduced in Ref. [19] to solve the AWB equation numerically. Our numerical results match the analytic results obtained in Sec. IV when the Chapman-Enskog expressions for the transport coefficients are employed. For completeness, a short description of the numerical method is provided in Appendix A. In order to better understand the rarefaction effects that appear at large values of the relaxation time  $\tau$ , we also discuss the longitudinal wave problem in the free-streaming limit in Sec. VI. We present our conclusions in Sec. VII.

Throughout this paper, we use the metric convention  $\eta_{\mu\nu} = \text{diag}(-1, 1, 1, 1)$  and Planck units, such that  $c = \hbar = K_B = 1$ .

## II. RELATIVISTIC KINETIC THEORY

In this paper, we will focus on the relativistic Boltzmann equation for massless particles in the Anderson-Witting approximation for the collision term:

$$p^\mu \partial_\mu f = \frac{p \cdot u_L}{\tau} (f - f_L^{(\text{eq})}), \quad (2.1)$$

where we assume for simplicity that the relaxation time  $\tau$  is constant. The equilibrium distribution  $f^{(\text{eq})}$  is taken to be the Maxwell-Jüttner distribution function:

$$f_L^{(\text{eq})} = \frac{n_L}{8\pi T_L^3} \exp\left(\frac{p \cdot u_L}{T_L}\right). \quad (2.2)$$

In the above,  $n_L$  represents the particle number density,  $u_L^\mu$  is the macroscopic four-velocity,  $T_L$  is the local temperature and  $p^\mu$  is the on-shell particle four-momentum. The quantities bearing the subscript  $L$  are expressed in the Landau frame [28].

The transition from the Boltzmann equation (2.1) to relativistic hydrodynamics is done by defining the macroscopic four-flow vector  $N^\mu$  and stress-energy tensor  $T^{\mu\nu}$  by integrating the distribution function over the momentum space:

$$N^\mu = \int \frac{d^3p}{p^0} f p^\mu, \quad T^{\mu\nu} = \int \frac{d^3p}{p^0} f p^\mu p^\nu. \quad (2.3)$$

Multiplying the Boltzmann equation (2.1) by the collision invariants  $\psi \in \{1, p^\mu\}$  and integrating with respect to the momentum space, the following conservation equations are obtained:

$$\partial_\mu N^\mu = 0, \quad \partial_\nu T^{\mu\nu} = 0. \quad (2.4)$$

Due to its simplicity and pedagogical value, we will work in this paper in the Eckart frame, where the macroscopic velocity  $u^\mu$  is defined as the unit vector parallel to  $N^\mu$  [29, 30]:

$$u^\mu = N^\mu / \sqrt{-N^2}. \quad (2.5)$$

With respect to  $u^\mu$ ,  $N^\mu$  and the stress-energy tensor (SET)  $T^{\mu\nu}$  can be decomposed as:

$$\begin{aligned} N^\mu &= n u^\mu, \\ T^{\mu\nu} &= E u^\mu u^\nu + (P + \bar{\omega}) \Delta^{\mu\nu} + u^\mu q^\nu + q^\nu u^\mu + \Pi^{\mu\nu}, \end{aligned} \quad (2.6)$$

where  $\Delta^{\mu\nu} = \eta^{\mu\nu} + u^\mu u^\nu$  is the projector on the hypersurface orthogonal to  $u^\mu$ . The particle number density  $n$ , energy density  $E$ , isotropic pressure  $P + \bar{\omega}$ , heat flux  $q^\mu$  and shear stress tensor  $\Pi^{\mu\nu}$  can be obtained as follows [26, 30]:

$$\begin{aligned} n &= -u_\mu N^\mu, \quad E = u_\mu u_\nu T^{\mu\nu}, \quad P = \frac{1}{3} \Delta_{\mu\nu} T^{\mu\nu}, \\ \Pi^{\mu\nu} &= \left( \Delta^\mu{}_\lambda \Delta^\nu{}_\kappa - \frac{1}{3} \Delta^{\mu\nu} \Delta_{\lambda\kappa} \right) T^{\lambda\kappa}, \\ q^\mu &= -\Delta^\mu{}_\nu u_\lambda T^{\nu\lambda}, \end{aligned} \quad (2.7)$$

while the dynamic pressure  $\overline{\omega} = 0$  for massless particles, when  $E = 3P$ .

The system (2.4) consisting of 5 equations is not closed. For simplicity, we restrict the analysis presented in this paper to the so-called five-field theory, where  $q^\mu$  and  $\Pi^{\mu\nu}$  are given in terms of the fundamental variables  $n$ ,  $u^\mu$  and the temperature  $T = P/n$  via the following constitutive equations [1, 30]:

$$\begin{aligned} q^\mu &= -\lambda \Delta^{\mu\nu} \left( \partial_\nu T - \frac{T}{E+P} \partial_\nu P \right), \\ \Pi^{\mu\nu} &= -\eta \left[ (\Delta^{\mu\lambda} \Delta^{\nu\kappa} + \Delta^{\nu\lambda} \Delta^{\mu\kappa}) - \frac{2}{3} \Delta^{\mu\nu} \Delta^{\lambda\kappa} \right] \partial_\lambda u_\kappa. \end{aligned} \quad (2.8)$$

The coefficients of heat conductivity  $\lambda$  and shear viscosity  $\eta$  represent the transport coefficients which make the object of the present study. It is worth mentioning that the five-field theory is non-causal, since the ensuing system of equations is not hyperbolic [30]. This issue can be remedied by considering higher-order extensions, such as the second order [30] or third order hydrodynamics [31, 32]. For simplicity, the analysis presented in this paper is limited to the five field theory.

The connection between the Boltzmann equation (2.1) and the constitutive equations (2.8) is commonly achieved via two paths: (a) the Chapman-Enskog expansion; and (b) Grad's 14 moments approximation. In the ultrarelativistic regime considered in this paper, the transport coefficients  $\eta$  and  $\lambda$  are given by:

$$\eta = \eta_0 P \tau, \quad \lambda = \lambda_0 n \tau, \quad (2.9)$$

where the dimensionless constants  $\eta_0$  and  $\lambda_0$  are obtained using Grad's approximation and the Chapman-Enskog procedure as follows:

$$\text{Grad method:} \quad \eta_{0,G} = \frac{2}{3}, \quad \lambda_{0,G} = \frac{4}{5}, \quad (2.10a)$$

$$\text{Chapman-Enskog :} \quad \eta_{0,C-E} = \frac{4}{5}, \quad \lambda_{0,C-E} = \frac{4}{3}. \quad (2.10b)$$

The validity of the constitutive equations (2.8) and of the above expressions for the transport coefficients is limited to the hydrodynamic regime, where  $\tau \lesssim 10^{-3}$ .

### III. LINEARISED RELATIVISTIC HYDRODYNAMICS

We now consider a system which is homogeneous along the  $x$  and  $y$  directions. Without loss of generality,  $u^\mu$ ,  $q^\mu$  and  $\Pi^{\mu\nu}$  can be taken as follows [19, 26]:

$$u = \gamma(\partial_t + \beta\partial_z), \quad q = q(\beta\partial_t + \partial_z),$$

$$\Pi^{\mu\nu} = \Pi \begin{pmatrix} \beta^2\gamma^2 & 0 & 0 & \beta\gamma^2 \\ 0 & -\frac{1}{2} & 0 & 0 \\ 0 & 0 & -\frac{1}{2} & 0 \\ \beta\gamma^2 & 0 & 0 & \gamma^2 \end{pmatrix}, \quad (3.1)$$

where  $\gamma = (1 - \beta^2)^{-1/2}$  is the Lorentz factor corresponding to the velocity  $\beta$ .

We now consider a flow where  $\beta \ll 1$ , such that the terms of order  $\beta^2$  can be neglected. Furthermore, we consider small perturbations  $\delta n$  and  $\delta P$  around the background density  $n_0$  and pressure  $P_0$ , respectively. In this approximation, the constitutive equations (2.8) reduce to:

$$q = -\frac{\lambda P_0}{4n_0} \left( \frac{3}{P_0} \partial_z \delta P - \frac{4}{n_0} \partial_z \delta n \right), \quad \Pi = -\frac{4\eta}{3} \partial_z \beta. \quad (3.2)$$

Since  $q$  and  $\Pi$  are already of first order in the perturbations  $\beta$ ,  $\delta n$  and  $\delta P$ , the only non-negligible components of  $q^\mu$  and  $\Pi^{\mu\nu}$  are  $q^z = q$  and  $\Pi^{zz} \simeq -2\Pi^{xx} = -2\Pi^{yy} = \Pi$ . Thus, the conservation equations (2.4) reduce to:

$$\begin{aligned} \partial_t \delta n + n_0 \partial_z \beta &= 0, \\ 3\partial_t \delta P + 4P_0 \partial_z \beta + \partial_z q &= 0, \\ 4P_0 \partial_t \beta + \partial_t q + \partial_z \delta P + \partial_z \Pi &= 0. \end{aligned} \quad (3.3)$$

### IV. LONGITUDINAL WAVES

We now seek solutions of the form:

$$\begin{pmatrix} \beta \\ q \end{pmatrix} = \sin kz \begin{pmatrix} \beta_\alpha \\ q_\alpha \end{pmatrix} e^{-\alpha t},$$

$$\begin{pmatrix} \delta n \\ \delta P \\ \Pi \end{pmatrix} = \cos kz \begin{pmatrix} \delta n_\alpha \\ \delta P_\alpha \\ \Pi_\alpha \end{pmatrix} e^{-\alpha t}, \quad (4.1)$$

where  $k = 2\pi/L$  is the wave number and  $L$  is the wavelength. The imaginary part of the coefficient  $\alpha$  represents the propagation frequency, while its real part causes the dissipative dampening of the wave. In the above,  $q_\alpha$  and  $\Pi_\alpha$  can be found from Eqs. (3.2):

$$q_\alpha = \frac{k\lambda P_0}{4n_0} \left( 3\frac{\delta P_\alpha}{P_0} - 4\frac{\delta n_\alpha}{n_0} \right), \quad \Pi_\alpha = -\frac{4k\eta}{3}\beta_\alpha. \quad (4.2)$$

Substituting Eqs. (4.1) and (4.2) into Eq. (3.3) yields the following system of equations:

$$\begin{aligned} \alpha\delta n_\alpha - kn_0\beta_\alpha &= 0, \\ 3\alpha\delta P_\alpha - 4kP_0\beta_\alpha - kq_\alpha &= 0, \\ 4\alpha P_0\beta_\alpha + \alpha q_\alpha + k\delta P_\alpha + k\Pi_\alpha &= 0. \end{aligned} \quad (4.3)$$

The above equations admit the following solutions for  $\alpha$ :

$$\alpha_\lambda = \frac{k^2\lambda}{4n_0}, \quad \alpha_\pm = \alpha_d \pm i\alpha_o, \quad (4.4)$$

where the dampening ( $\alpha_d$ ) and oscillatory ( $\alpha_o$ ) parts of  $\alpha_\pm$  read:

$$\alpha_d = \frac{k^2\eta}{6P_0}, \quad \alpha_o = \frac{k}{\sqrt{3}}\sqrt{1 - \frac{3\alpha_d^2}{k^2}}, \quad (4.5)$$

It is worth noting that the phase velocity  $\alpha_o/k = c_s\sqrt{1 - \frac{3\alpha_d^2}{k^2}}$  is smaller than the sound speed  $c_s = 1/\sqrt{3}$ . The amplitudes of the density and pressure perturbations  $\delta n_\alpha$  and  $\delta P_\alpha$  are given in terms of the velocity amplitudes  $\beta_\lambda$  and  $\beta_\pm$  corresponding to  $\alpha_\lambda$  and  $\alpha_\pm$  as follows:

$$\begin{aligned} \delta n_\lambda &= \frac{kn_0\beta_\lambda}{\alpha_\lambda}, & \delta P_\lambda &= \frac{8P_0\alpha_d}{k} \frac{\beta_\lambda}{1 + (3\alpha_\lambda^2/k^2)}, \\ \delta n_\pm &= \frac{kn_0}{\alpha_\pm}\beta_\pm, & \delta P_\pm &= \frac{4kP_0}{3\alpha_\pm}\beta_\pm. \end{aligned} \quad (4.6)$$

The general solution of Eq. (3.3) can thus be written as:

$$\beta = \tilde{\beta} \sin kz, \quad \delta n = \tilde{\delta n} \cos kz, \quad \delta P = \tilde{\delta P} \cos kz, \quad (4.7)$$

where the quantities with a tilde depend only on time:

$$\begin{pmatrix} \tilde{\beta} \\ \tilde{\delta n} \\ \tilde{\delta P} \end{pmatrix} = \begin{pmatrix} \beta_\lambda \\ \delta n_\lambda \\ \delta P_\lambda \end{pmatrix} e^{-\alpha_\lambda t} + \left[ \begin{pmatrix} \beta_c \\ \delta n_c \\ \delta P_c \end{pmatrix} \cos \alpha_o t + \begin{pmatrix} \beta_s \\ \delta n_s \\ \delta P_s \end{pmatrix} \sin \alpha_o t \right] e^{-\alpha_d t}. \quad (4.8)$$



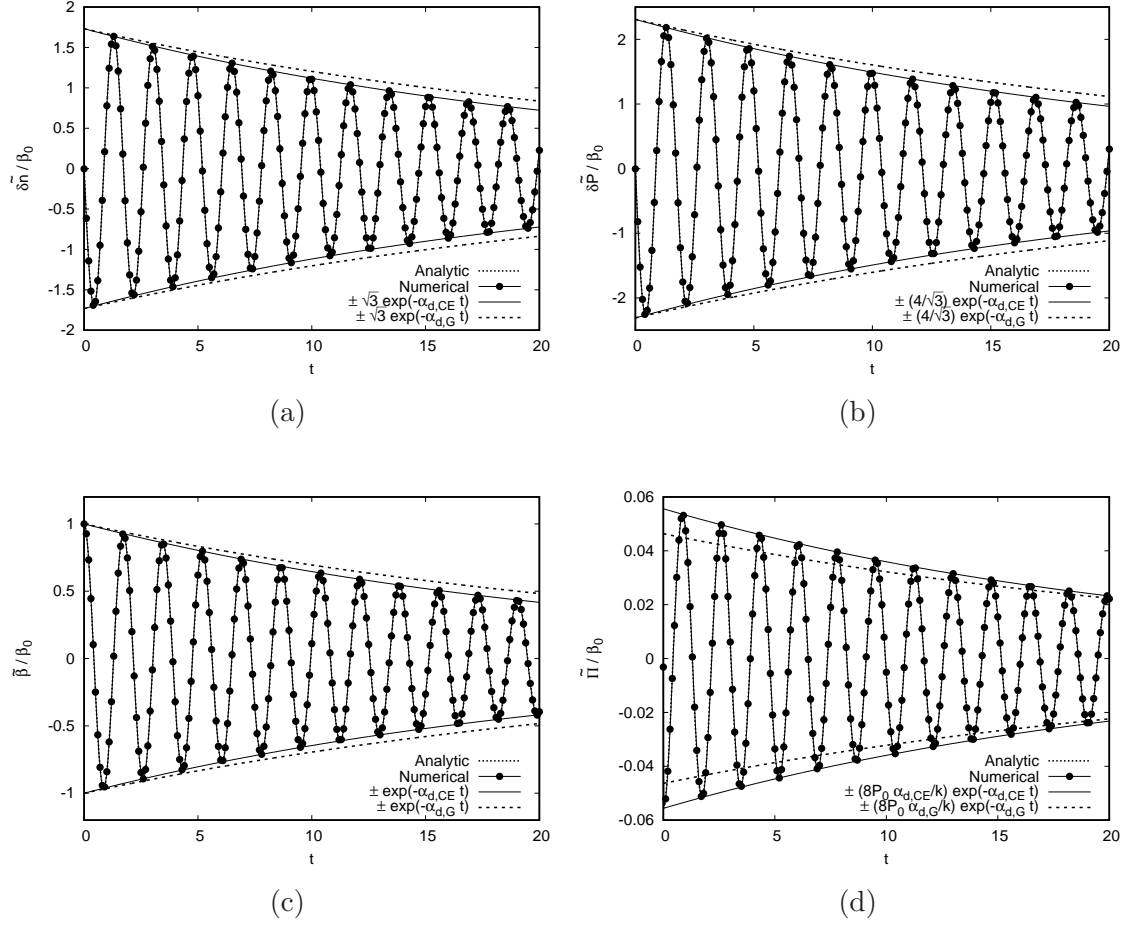


FIG. 1. Comparison between the analytic solutions in Eq. (4.16) and the numerical results obtained at  $\tau = 8.3 \times 10^{-3}$ . The vertical axes represents the values of (a)  $\widetilde{\delta n}$ , (b)  $\widetilde{\delta P}$ , (c)  $\widetilde{\beta}$  and (d)  $\widetilde{\Pi}$ , divided by  $\beta_0$ . The coefficient  $\alpha_d$  in the asymptotic dampening lines is given in Eq. (4.5), while  $\alpha_o \simeq k\sqrt{3}$ . The system was initialised according to *Case 1* of Sec. V, i.e.  $\delta n_0 = \delta P_0 = 0$  and  $\beta_0 = 10^{-3}$ .

In the above,  $\beta_\lambda$ ,  $\beta_c = \beta_+ + \beta_-$  and  $\beta_s = -i(\beta_+ - \beta_-)$  are independent integration constants with respect to which we have defined:

$$\begin{aligned} \begin{pmatrix} \delta n_c \\ \delta P_c \end{pmatrix} &= \begin{pmatrix} kn_0 \\ 4kP_0/3 \end{pmatrix} \frac{\alpha_d \beta_c + \alpha_o \beta_s}{\alpha_d^2 + \alpha_o^2}, \\ \begin{pmatrix} \delta n_s \\ \delta P_s \end{pmatrix} &= \begin{pmatrix} kn_0 \\ 4kP_0/3 \end{pmatrix} \frac{\alpha_d \beta_s - \alpha_o \beta_c}{\alpha_d^2 + \alpha_o^2}, \end{aligned} \quad (4.9)$$

while  $\delta n_\lambda$  and  $\delta P_\lambda$  were already defined in Eq. (4.6). Since  $3n_0\delta P_\pm - 4P_0\delta n_\pm = 0$ , the heat

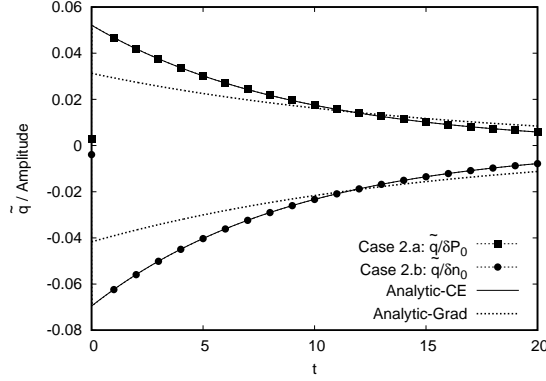


FIG. 2. Time dependence of  $\tilde{q}$  for the initialisation corresponding to *Case 2 (a)* (i.e.  $\delta n_0 = \beta_0 = 0$  and  $\delta P_0 = 10^{-3}$ ) and *Case 2 (b)* (i.e.  $\delta P_0 = \beta_0 = 0$  and  $\delta n_0 = 10^{-3}$ ). The dotted lines with points represent the numerical results. The analytic solution (4.17) is represented for the two cases using solid lines when  $\alpha_\lambda$  is computed using the Chapman-Enskog expression for  $\lambda$  (2.10b), while the dotted lines correspond to the case when the Grad expression (2.10a) is used. The relaxation time for the numerical simulations was set to  $\tau = 0.0083$ .

flux does not possess an oscillatory term, such that  $q$  reduces to:

$$q = \tilde{q} \sin kz, \quad \tilde{q} = q_\lambda e^{-\alpha_\lambda t}, \quad (4.10)$$

where  $q_\lambda$  can be obtained by substituting  $\delta n_\lambda$  and  $\delta P_\lambda$  into Eq. (4.2). The constants  $\beta_\lambda$ ,  $\beta_c$  and  $\beta_s$  can be obtained by imposing the following initial conditions:

$$\beta(t=0) = \beta_0 \sin kz, \quad \begin{pmatrix} \delta n \\ \delta P \end{pmatrix}_{t=0} = \begin{pmatrix} \delta n_0 \\ \delta P_0 \end{pmatrix} \cos kz, \quad (4.11)$$

where

$$\beta_0 = \beta_\lambda + \beta_c, \quad \delta n_0 = \delta n_\lambda + \delta n_c, \quad \delta P_0 = \delta P_\lambda + \delta P_c. \quad (4.12)$$

The solution of Eqs. (4.12) can be written as:

$$\begin{aligned} \beta_c &= \beta_0 + \frac{\alpha_\lambda(k^2 + 3\alpha_\lambda^2)}{4k[k^2 + 3\alpha_\lambda(\alpha_\lambda - 2\alpha_d)]} \left( \frac{3\delta P_0}{P_0} - \frac{4\delta n_0}{n_0} \right), \\ \beta_s &= -\frac{\alpha_d}{\alpha_o} \beta_c + \frac{3(\alpha_d^2 + \alpha_o^2)}{4k\alpha_o[k^2 + 3\alpha_\lambda(\alpha_\lambda - 2\alpha_d)]} \\ &\quad \times \left[ (k^2 + 3\alpha_\lambda^2) \frac{\delta P_0}{P_0} - 8\alpha_d\alpha_\lambda \frac{\delta n_o}{n_o} \right], \\ \beta_\lambda &= -\frac{\alpha_\lambda(k^2 + 3\alpha_\lambda^2)}{4k[k^2 + 3\alpha_\lambda(\alpha_\lambda - 2\alpha_d)]} \left( \frac{3\delta P_0}{P_0} - \frac{4\delta n_0}{n_0} \right), \end{aligned} \quad (4.13)$$

such that  $q_\lambda$  (4.2) becomes:

$$q_\lambda = \frac{\alpha_\lambda P_0}{k} \left( \frac{3\delta P_0}{P_0} - \frac{4\delta n_0}{n_0} \right). \quad (4.14)$$

*a. Case 1: Adiabatic flow* First, we consider an adiabatic flow (i.e.  $q = 0$ ) such that the shear viscosity  $\eta$  can be isolated from the heat conductivity  $\lambda$ . This can be achieved when  $3n_0\delta P_0 = 4P_0\delta n_0$ . This condition is equivalent to the requirement that the fugacity  $\lambda_{\text{fug}} = n^4/P^3$  remains constant, i.e.  $\delta\lambda_{\text{fug}} = 0$ . Moreover, Eq. (4.13) indicates that, when  $3n_0\delta P_0 = 4P_0\delta n_0$ ,  $\beta_\lambda = 0$ , while Eqs. (4.6), (4.14) and (4.2) imply that  $\delta n_\lambda$ ,  $\delta P_\lambda$ ,  $q_\lambda$  and  $\Pi_\lambda$  cancel. Thus, the evolution of the fluid is completely independent of  $\alpha_\lambda$ , enabling the shear viscosity to be determined independently.

For simplicity, we set  $\delta n_0 = \delta P_0 = 0$ , such that Eqs. (4.13) become:

$$\beta_c = \beta_0, \quad \beta_s = -\frac{\alpha_d}{\alpha_o}\beta_0, \quad \beta_\lambda = 0. \quad (4.15)$$

The exact solution reads:

$$\begin{aligned} \begin{pmatrix} \widetilde{\beta} \\ \widetilde{\Pi} \end{pmatrix} &= \beta_0 \left( \cos \alpha_o t - \frac{\alpha_d}{\alpha_o} \sin \alpha_o t \right) \begin{pmatrix} 1 \\ -8P_0\alpha_d/k \end{pmatrix} e^{-\alpha_d t}, \\ \widetilde{\delta n} &= -\frac{kn_0\beta_0}{\alpha_o} e^{-\alpha_d t} \sin \alpha_o t, \\ \widetilde{\delta P} &= -\frac{4kP_0\beta_0}{3\alpha_o} e^{-\alpha_d t} \sin \alpha_o t, \end{aligned} \quad (4.16)$$

where  $\alpha_d$  and  $\alpha_o$  are given in terms of  $\eta$  in Eq. (4.5).

*b. Case 2, (a) and (b): Non-adiabatic flow* The coefficient  $\alpha_\lambda$  can be investigated most easily by considering the decay of the heat flux (4.10). For simplicity, we choose the cases when (a)  $\delta n_0 = \beta_0 = 0$ ; and when (b)  $\delta P_0 = \beta_0 = 0$ , such that Eq. (4.10) becomes:

$$\widetilde{q} = \frac{\alpha_\lambda P_0}{k} \left( \frac{3\delta P_0}{P_0} - \frac{4\delta n_0}{n_0} \right) e^{-\alpha_\lambda t}, \quad (4.17)$$

while the coefficients  $\beta_c = -\beta_\lambda$  and  $\beta_s$  can be found from Eqs. (4.13).

## V. NUMERICAL ANALYSIS

The analytic solution discussed in the previous section facilitates the study of the transport coefficients corresponding to a relativistic gas. Using the numerical method described in A, we will consider this system for the study of the ultrarelativistic limit of the shear viscosity  $\eta$  and heat conductivity  $\lambda$  arising from the relativistic Boltzmann equation in the Anderson-Witting approximation.

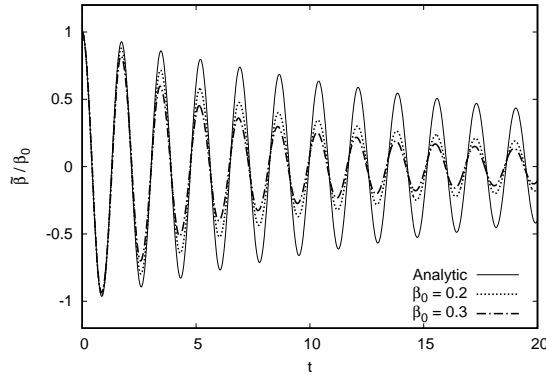


FIG. 3. The ratio  $\tilde{\beta}/\beta_0$  for various values of  $\beta_0$  corresponding to *Case 1* presented in Sec. V. As  $\beta_0$  increases, the time evolution of  $\tilde{\beta}/\beta_0$  departs from the solution (4.16), indicating that non-linear effects become important.

#### A. Chapman-Enskog vs. Grad

In Fig. 1, the time evolutions of  $\tilde{\beta}$ ,  $\tilde{\delta n}$ ,  $\tilde{\delta P}$  and  $\tilde{\Pi}$  are presented for the initial conditions corresponding to *Case 1*, namely  $\delta n_0 = \delta P_0 = 0$  and  $\beta_0 = 10^{-3}$ . The relaxation time was taken to be  $\tau = 0.0083$ . The first entry in the legend (fine dotted lines) correspond to the analytic expressions in Eqs. (4.16), where  $\alpha_d$  and  $\alpha_o$  are computed using the Chapman-Enskog value for  $\eta$ . The numerical results are indistinguishable from the analytic predictions.

Also in the plots in Fig. 1, the dampening caused by the  $\exp(-\alpha_d t)$  factor in Eqs. (4.16) is represented when  $\alpha_d$  is calculated using the Chapman-Enskog and Grad expressions for  $\eta$ . The amplitude of the dampening term in the case of  $\tilde{\beta}/\beta_0$  is approximated as  $\sqrt{1 + \alpha_d^2/\alpha_o^2} \simeq 1$ , and similarly in the case of  $\tilde{\Pi}/\beta_0$ . It can be seen that the dampening predicted by the analytic solution when the Grad expression for  $\eta$  is used does not match the numerical results.

Next, Fig. 2 shows a comparison between the analytic prediction for  $\tilde{q}$  in the frame of *Case 2* and our numerical results. The plot contains results for the cases when the system is initialised with (a)  $\delta n_0 = 0$  and  $\delta P_0 = 10^{-3}$  or (b)  $\delta P_0 = 0$  and  $\delta n_0 = 10^{-3}$ . For each of these cases, three curves are represented. Our numerical results (represented using dashed lines and points) are overlapped with the analytic prediction (4.17) when  $\alpha_\lambda$  is calculated the Chapman-Enskog expression for  $\lambda$  (represented by a continuous line). The analytic

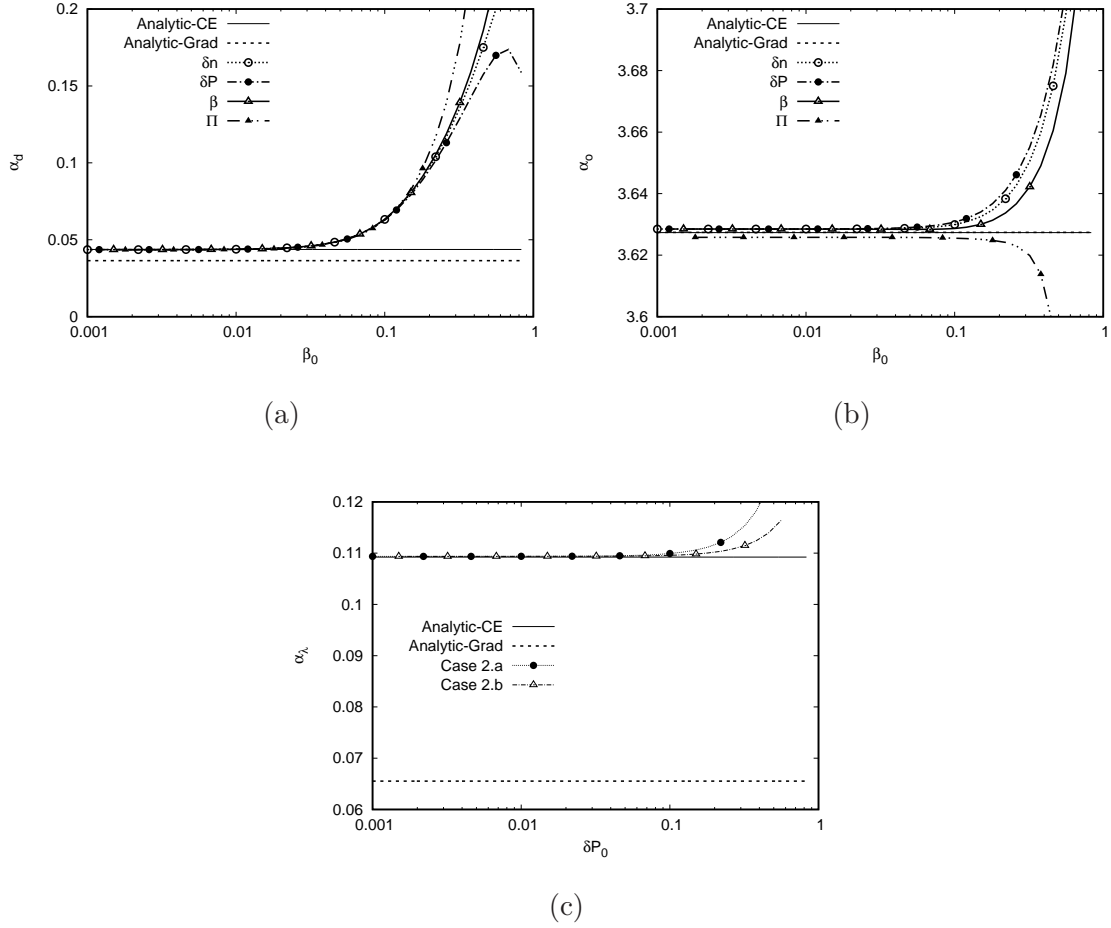


FIG. 4. The dependence of (a)  $\alpha_d$  and (b)  $\alpha_o$  on  $\beta_0$ ; the four curves correspond to the two-parameter non-linear fit of  $\widetilde{\delta n}$ ,  $\widetilde{\delta P}$ ,  $\widetilde{\beta}$  and  $\widetilde{\Pi}$  of the numerical data corresponding to Eq. (4.16). (c) The dependence of  $\alpha_\lambda$  on the amplitude of the initial perturbation, namely on  $\delta P_0$  and  $\delta n_0$  for the initial conditions of *Case 2(a)* and *Case 2(b)*, respectively. The fit is performed on  $\widetilde{q}$  by considering the analytic solution in Eq. (4.17). The relaxation time was always kept at  $\tau = 0.0083$ .

prediction (4.17) corresponding to the case when  $\alpha_\lambda$  is obtained using the Grad expression for  $\lambda$  is clearly not consistent with our numerical results. The points at  $t \simeq 0$  indicate that we have initialised the system using an equilibrium state, in which the heat flux vanishes. This is to be contrasted with the result in Eq. (4.17), where  $\widetilde{q}(t = 0) \neq 0$ . However, since  $\tau$  is small, the system quickly relaxes towards the analytic prediction (4.17).

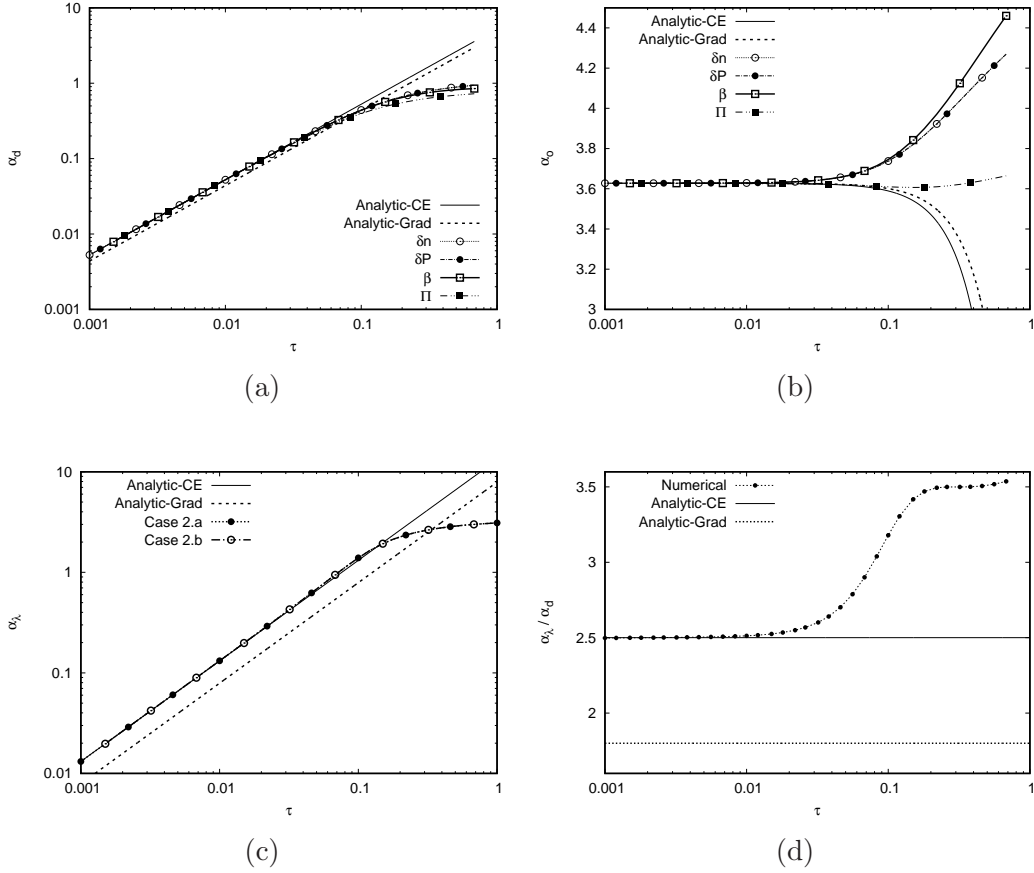


FIG. 5. Graphical representation of the dependence of (a)  $\alpha_d$ , (b)  $\alpha_o$ , (c)  $\alpha_\lambda$  and (d) the ratio  $\alpha_\lambda/\alpha_d$  on  $\tau$ . On each plot, the analytic curves corresponding to the Chapman-Enskog and Grad methods are displayed. The numerical results for the coefficients  $\alpha_d$  and  $\alpha_o$  are obtained using a two-parameter non-linear fit performed on the numerical results for  $\widetilde{\delta n}$ ,  $\widetilde{\beta}$ ,  $\widetilde{\delta P}$  and  $\widetilde{\Pi}$  with the initial conditions corresponding to *Case 1*, namely  $\delta n_0 = \delta P_0 = 0$  and  $\beta_0 = 10^{-3}$ . The numerical curves for the coefficient  $\alpha_\lambda$  are obtained by performing a one-parameter non-linear fit on  $\widetilde{q}$  with the initial conditions described in *Case 2*, namely  $\beta_0 = 0$  and either  $\delta n_0 = 0$  and  $\delta P_0 = 10^{-3}$  (*Case 2.a*) or  $\delta P_0 = 0$  and  $\delta n_0 = 10^{-3}$  (*Case 2.b*). In (d),  $\alpha_d$  and  $\alpha_\lambda$  are obtained using a nonlinear fit on  $\widetilde{\beta}$  (*Case 1*) and  $\widetilde{q}$  (*Case 2.a*), respectively.

## B. Limits of the linearised hydrodynamics equations

We now test the limits in which the solution of the linearised equations (3.3) are applicable. In order to reduce the rarefaction effects, we fix  $\tau = 0.0083$  throughout this subsection.

The solution (4.16) predicts that the time evolution of  $\tilde{\beta}$  is damped according to  $\exp(-\alpha_d)$ , while  $\alpha_d$  (4.5) does not depend on the magnitude  $\beta_0$  of the perturbation. Figure 3 shows that this is not the case: while at small values of  $\tau$ ,  $\tilde{\beta}$  follows closely the analytic prediction [as confirmed in Fig. 1(c)], at larger values of  $\beta$ , the dampening is enhanced compared to the hydrodynamic limit (4.5). Indeed, the dampening of  $\tilde{\beta}$  is stronger when  $\beta_0 = 0.3$  than when  $\beta_0 = 0.2$ , which in turn is stronger than in the hydrodynamic regime.

The dependence of  $\alpha_d$ ,  $\alpha_o$  and  $\alpha_\lambda$  on the amplitude of the perturbations is presented in Fig. 4(a) and Fig. 4(b). The coefficients  $\alpha_d$  and  $\alpha_o$  are obtained from the numerical results corresponding to the initial conditions of *Case 1*, i.e.  $\delta n_0 = \delta P_0 = 0$  and various values of  $\beta_0$ . The coefficient  $\alpha_\lambda$  [represented in Fig. 4(c)] is obtained in the context of *Case 2*, i.e. when  $\beta_0 = 0$  and (a)  $\delta n_0 = 0$  or (b)  $\delta P_0 = 0$ . The horizontal axis in Fig. 4(c) represents the amplitude of the initial perturbation, i.e.  $\delta P_0$  for *Case 2(a)* and  $\delta n_0$  for *Case 2(b)*. All of the above plots show the analytic predictions (4.5) and (4.4) for  $\alpha_d$ ,  $\alpha_o$  and  $\alpha_\lambda$ , specialised to the cases when the transport coefficients  $\eta$  and  $\lambda$  are computed using the Chapman-Enskog (2.10b) and the Grad (2.10a) expressions. The results clearly favour the Chapman-Enskog expressions. It is also evident from these plots that the analytic analysis performed in Sec. III in the context of the linearised hydrodynamic equations loses applicability when the perturbation amplitude is larger than  $\sim 0.1$ .

### C. Limits of the hydrodynamic regime

Next, we focus on the validity of the analysis presented in Sec. III as the relaxation time  $\tau$  is increased. In particular, it is known that the constitutive equations (2.4) are valid only when  $\tau$  is small [1].

In order to test the effect of increasing  $\tau$ , we keep the perturbations small, i.e.  $\beta_0 = 0.001$  (for *Case 1*),  $\delta P_0 = 0.001$  [for *Case 2(a)*], or  $\delta n_0 = 0.001$  [for *Case 2(b)*]. The plots in Fig. 5 show the dependence of (a)  $\alpha_d$ , (b)  $\alpha_o$ , (c)  $\alpha_\lambda$  and (d) the ratio  $\alpha_\lambda/\alpha_d$  on the value of  $\tau$ . As before, the analytic predictions for the dependence of these coefficients on  $\tau$  is also shown for the cases when the transport coefficients  $\eta$  and  $\lambda$  are obtained using the Chapman-Enskog (2.10b) and Grad (2.10a) expressions. For  $\tau < 0.1$ , our numerical results clearly favour the Chapman-Enskog expression. Plot (d) confirms that for small values of  $\tau$ , the ratio  $\lambda/\eta = 2\alpha_\lambda n_0/3\alpha_\eta P_0$  is equal to  $5/3$ , as predicted in the Chapman-Enskog theory (2.10b).

This value is in agreement with the high chemical potential limit of Fig. 2 in Ref. [33]

While for  $\tau \gtrsim 0.1$ , the constitutive equations (2.4) no longer hold, our non-linear fit analysis seems to indicate that the dampening coefficients  $\alpha_d$  and  $\alpha_\lambda$  plateau at large  $\tau$ . This conclusion is not necessarily meaningful, since the ansatz (4.1) that the time dependence of  $\delta n$ ,  $\delta P$  and  $\beta$  is of the form  $e^{-\alpha t}$  with constant  $\alpha$  is not guaranteed to be valid in the transition regime. It is certain that the time dependence of the above quantities is more complex, since the dissipative dampening is absent in the ballistic regime, as will be discussed in Sec. VI.

## VI. THE BALLISTIC LIMIT

For completeness, we end our analysis of the longitudinal wave problem by considering the free-streaming limit. In this case, the relativistic Boltzmann equation (2.1) reduces to:

$$\partial_t f + \xi \partial_z f = 0, \quad (6.1)$$

where  $\xi = p^z/p$ . The solution of Eq. (6.1) is  $f(z, \xi, t) = f(z - \xi t)$ , subject to the following initial condition:

$$f(z, \xi, t = 0) = \frac{n(z)}{8\pi T^3(z)} \exp \left\{ -\frac{p\gamma(z)}{T(z)} [1 - \xi \beta(z)] \right\}. \quad (6.2)$$

We now consider the case of the longitudinal wave, where:

$$\begin{aligned} n(z) &= n_0 + \delta n_0 \cos kz, & P(z) &= P_0 + \delta P_0 \cos kz, \\ \beta(z) &= \beta_0 \sin kz. \end{aligned} \quad (6.3)$$

Assuming that  $\delta n_0$ ,  $\delta P_0$  and  $\beta_0$  are small, Eq. (6.2) can be linearised as follows:

$$\begin{aligned} f(z, \xi, t = 0) &\simeq \frac{n_0}{8\pi T_0^3} e^{-p/T_0} \left\{ 1 + \frac{p\xi}{T_0} \beta_0 \sin kz \right. \\ &\quad \left. \left[ \frac{4\delta n_0}{n_0} - \frac{3\delta P_0}{P_0} + \frac{p}{T_0} \left( \frac{\delta P_0}{P_0} - \frac{\delta n_0}{n_0} \right) \right] \cos kz \right\}. \end{aligned} \quad (6.4)$$

At  $t > 0$ , the product  $kz$  in the trigonometric functions is replaced by  $k(z - \xi t)$ .

We are interested in tracking the time evolution of the macroscopic quantities  $n$ ,  $P$ ,  $\beta$ ,  $q$  and  $\Pi$ . These can be obtained from  $N^\mu$  and  $T^{\mu\nu}$  (2.3), which reduce to:

$$\begin{aligned} N^\mu(t, z) &= \int_0^\infty dp p^2 \int d\Omega v^\mu f(z - \xi t), \\ T^{\mu\nu}(t, z) &= \int_0^\infty dp p^3 \int d\Omega v^\mu v^\nu f(z - \xi t), \end{aligned} \quad (6.5)$$



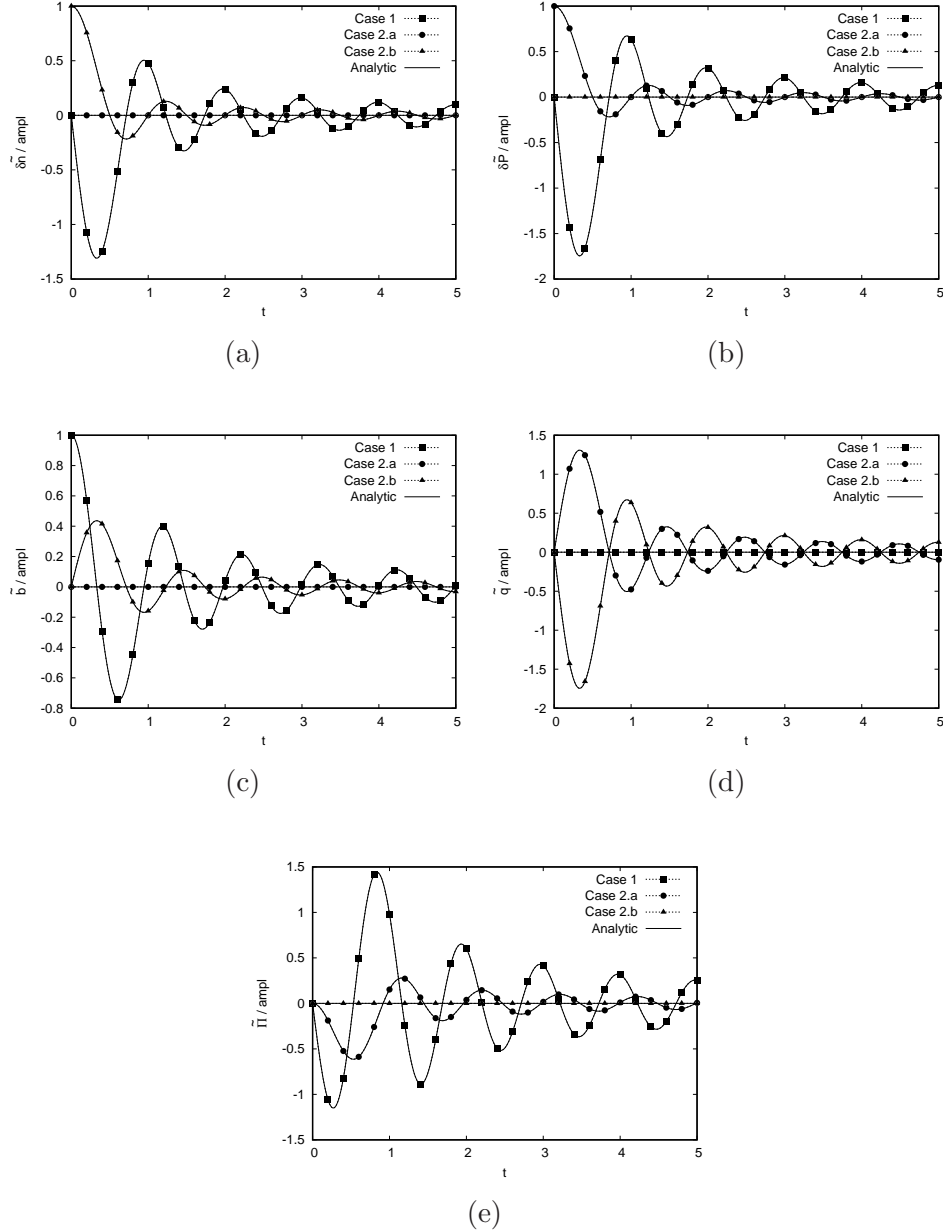


FIG. 6. Time evolution of (a)  $\widetilde{\delta n}$ , (b)  $\widetilde{\delta P}$ , (c)  $\widetilde{\beta}$ , (d)  $\widetilde{q}$  and (e)  $\widetilde{\Pi}$  in the free-streaming regime, normalised with respect to the wave amplitude. The system is initialised with the following initial conditions: *Case 1*:  $\delta n_0 = \delta P_0 = 0$  and the wave amplitude is  $\beta_0 = 10^{-3}$ ; *Case 2(a)*:  $\delta n_0 = \beta_0 = 0$  and the wave amplitude is  $\delta P_0 = 10^{-3}$ ; *Case 2(b)*:  $\delta P_0 = \beta_0 = 0$  and the wave amplitude is  $\delta n_0 = 10^{-3}$ , such that the wave amplitude is always  $10^{-3}$ . The numerical results are represented with dashed lines and points, while the analytic results corresponding to Eq. (6.6) are represented using solid lines. The analytic and numerical curves are indistinguishable.

where  $v^\mu = p^\mu/p = (1, \sin \theta \cos \varphi, \sin \theta \sin \varphi, \cos \theta)$  and the integration measure is  $d^3p/p^0 = p dp d\Omega$ . The result is:

$$\begin{aligned}
\widetilde{n} &= \delta n_0 \frac{\sin kt}{kt} + 3\beta_0 n_0 \left[ \frac{\cos kt}{kt} - \frac{\sin kt}{(kt)^2} \right], \\
\widetilde{P} &= \delta P_0 \frac{\sin kt}{kt} + 4P_0 \beta_0 \left[ \frac{\cos kt}{kt} - \frac{\sin kt}{(kt)^2} \right], \\
\widetilde{\beta} &= -\frac{\delta n_0}{n_0} \left[ \frac{\cos kt}{kt} - \frac{\sin kt}{(kt)^2} \right] \\
&\quad + 3\beta_0 \left[ \frac{\sin kt}{kt} + \frac{2 \cos kt}{(kt)^2} - \frac{2 \sin kt}{(kt)^3} \right], \\
\widetilde{q} &= P_0 \left( \frac{4\delta n_0}{n_0} - \frac{3\delta P_0}{P_0} \right) \left[ \frac{\cos kt}{kt} - \frac{\sin kt}{(kt)^2} \right], \\
\widetilde{\Pi} &= 2\delta P_0 \left[ \frac{\sin kt}{kt} + \frac{3 \cos kt}{(kt)^2} - \frac{3 \sin kt}{(kt)^3} \right] \\
&\quad + 8P_0 \beta_0 \left[ \frac{\cos kt}{kt} - \frac{4 \sin kt}{(kt)^2} - \frac{9 \cos kt}{(kt)^3} + \frac{9 \sin kt}{(kt)^4} \right]. \tag{6.6}
\end{aligned}$$

The leading order term in all of the above expressions is damped according to a factor of  $t^{-1}$ .

Figure 6 illustrates the close agreement between our numerical method and the analytic solution (6.6). Each plot in Fig. 6 contains three curves corresponding to the initial conditions described in *Cases 1* ( $\delta n_0 = \delta P_0 = 0$ ,  $\beta_0 = 10^{-3}$ ), *2(a)* ( $\delta n_0 = \beta_0 = 0$ ,  $\delta P_0 = 10^{-3}$ ) and *2(b)* ( $\delta P_0 = \beta_0 = 0$ ,  $\delta n_0 = 10^{-3}$ ). The plots illustrate the time evolution of  $\widetilde{\delta n}$ ,  $\widetilde{\delta P}$ ,  $\widetilde{\delta b}$ ,  $\widetilde{q}$  and  $\widetilde{\Pi}$ , where our numerical results are represented with dashed lines and points, while the analytic expressions (6.6) are represented using solid lines. The quantities on the vertical axis are divided by the amplitude of the perturbation, namely  $\beta_0$  for *Case 1*,  $\delta P_0$  for *Case 2(a)* and  $\delta n_0$  for *Case 2(b)*. For simplicity, the amplitude was taken equal to  $10^{-3}$  in all cases. It can be seen that the agreement between our numerical results and the analytic expressions is excellent.

Each plot in Fig. 6 displays two non-trivial curves and a line corresponding to a vanishing value. This is because all of the expressions in Eq. (6.6) have on the right hand side only two terms, e.g.  $\widetilde{\delta n}$  vanishes when  $\delta n_0 = \beta_0 = 0$  for all values of  $\delta P_0$ , etc.

A fundamental difference between the hydrodynamic and the free-streaming regimes is that the attenuation of the wave perturbation in the former case is exponential, while in the latter case, it is of the form  $t^{-1}$ .

## VII. CONCLUSION AND OUTLOOK

In this paper, we provided numerical evidence that the ultrarelativistic limit of the transport coefficients corresponding to the Anderson-Witting approximation for the collision term in the relativistic Boltzmann equation is that predicted through the Chapman-Enskog procedure.

We arrived at the above conclusion by considering the attenuation of a longitudinal wave. For small values of the wave amplitude, the equations of dissipative hydrodynamics can be linearised and an analytic solution can be obtained in the context of the five-field approximation. The coefficient of shear viscosity  $\eta$  can be determined by considering a wave which propagates adiabatically. The coefficient of heat conductivity  $\lambda$  is determined by considering the dampening of the heat flux in the case when the wave propagates non-adiabatically.

Our analysis also shows that the hydrodynamic regime represented by the five-field theory provides an accurate description of the flow when the relaxation time  $\tau \lesssim 0.05$ . At the other end of the rarefaction spectrum, in the free-streaming limit, an analytic solution of the linearised regime indicates that the dampening of the initial (small) perturbation is polynomial (of the form  $t^{-1}$ ) instead of exponential. Our numerical method exactly reproduces the analytic solution in this regime.

We have also considered the case when the initial perturbation is not small. Our numerical experiments show that the solution of the linearised hydrodynamic equations in the five-field approximation is valid only when the amplitude of the initial perturbation is  $\lesssim 0.05$ .

We end this paper by noting that our hydrodynamic regime analysis based on the five-field theory is not fully compatible with our numerical simulations. Since in our numerical setup, we initialise the fluid in an equilibrium state, the heat flux  $q^\mu$  and pressure deviator  $\Pi^{\mu\nu}$  vanish everywhere at  $t = 0$ , regardless of the initial conditions for the density  $n$ , pressure  $P$  or velocity  $\beta$ . The five-field theory does not allow the initial conditions for  $q^\mu$  and  $\Pi^{\mu\nu}$  to be specified independently of  $n$ ,  $P$  and  $\beta$ . In order to increase the compatibility between the hydrodynamic flow description and our numerical setup within the kinetic theory framework, the first-order five-field description should be extended to the second-order 14-field dissipative hydrodynamics equations [30], or even the third-order equations [31, 32]. Such extensions can be used to measure the higher order transport coefficients

within the framework of the AWB equation. We hope to pursue this avenue of research in future publications.

## ACKNOWLEDGEMENTS

The author would like to thank Prof. Amaresh Jaiswal for useful discussions. This work was supported by a grant of the Romanian National Authority for Scientific Research and Innovation, CNCS-UEFISCDI, project number PN-II-RU-TE-2014-4-2910.

## Appendix A: Numerical method

In order to solve the AWB equation (2.1), the relativistic spherical lattice Boltzmann (R-SLB) models introduced in Ref. [19] are employed. A number of  $N = 100$  nodes are chosen along the  $z$  axis, where periodic boundary conditions apply, while the flow is assumed to be homogeneous along the  $x$  and  $y$  directions. The advection and time evolution are performed using the fifth-order weighted essentially non-oscillatory (WENO-5) [30] and third-order TVD Runge-Kutta (RK-3) [34] schemes, as presented in Ref. [19]. The lattice spacing is  $\delta z = 10^{-2}$  and the time step is  $\delta t = 10^{-3}$ .

The momentum space is factorised using spherical coordinates  $p$ ,  $\theta$  and  $\varphi$ , which are discretised using  $Q_L$ ,  $Q_\xi$  and  $Q_\varphi$  quadrature points, respectively. The quadrature order along the  $p$  direction is set to  $Q_L = 2$ , while the azimuthal quadrature order is  $Q_\varphi = 1$ . The model thus employs  $Q_L \times Q_\xi \times Q_\varphi = 2Q_\xi$  velocities.

The value of  $Q_\xi$  is chosen depending on the value of the relaxation time  $\tau$ . As discussed in Ref. [19],  $Q_\xi = 6$  is sufficient to obtain accurate results at  $\tau < 0.01$ . For values of  $\tau$  between 0.01 and 0.1, we set  $Q_\xi = 20$ , while for  $\tau \geq 0.1$ , we choose  $Q_\xi = 200$ .

The system is initialised with an equilibrium distribution  $f^{(\text{eq})}$  (2.2) at each point  $z_\ell = -0.5 + (\ell - \frac{1}{2})\delta z$ , truncated to  $N_L = 1$  and  $N_\Omega = 5$  with respect to  $p$  and  $\xi = \cos \theta$ , as explained in Ref. [19].

At a later time  $t_s = s \delta t$  ( $s = 1, 2, \dots 2.000$ ), the quantities with tilde defined in Eqs. (4.7)

are obtained as:

$$\begin{pmatrix} \widetilde{\beta}_s \\ \widetilde{q}_s \end{pmatrix} = 2\delta z \sum_{\ell=1}^N \begin{pmatrix} \beta_{s,\ell} \\ q_{s,\ell} \end{pmatrix} \sin kz_\ell, \\ \begin{pmatrix} \widetilde{\delta n}_s \\ \widetilde{\delta P}_s \\ \widetilde{\Pi}_s \end{pmatrix} = 2\delta z \sum_{\ell=1}^N \begin{pmatrix} n_{s,\ell} - n_0 \\ P_{s,\ell} - P_0 \\ \Pi_{s,\ell} \end{pmatrix} \cos kz_\ell. \quad (\text{A1})$$

The resulting values  $\widetilde{\beta}_s$ , etc. are stored at intervals of  $10\delta t = 0.01$ , resulting in a number of 2.000 values which are then further processed using Mathematica<sup>TM</sup> to obtain a nonlinear fit, based on the analytic solution for the flow.

For the flow considered in *Case 1*, the fit is performed based on the analytic solutions (4.16), where for each data set corresponding to  $\widetilde{\beta}$ ,  $\widetilde{\delta n}$ ,  $\widetilde{\delta P}$  and  $\widetilde{\Pi}$ , a fit is performed considering  $\alpha_d$  and  $\alpha_o$  as fitting parameters. For the flows considered in *Case 2(a)* and *(b)*, the fit is performed only for  $\widetilde{q}$  (4.17) with  $\alpha_\lambda$  as a fitting parameter.

It is worth mentioning that the non-equilibrium quantities  $q$  and  $\Pi$  vanish when  $f = f^{(\text{eq})}$ , such that the initial conditions for these quantities cannot be correctly imposed. Thus, the first 100 points (i.e. up to  $t = 1$ ) in each data set are excluded when performing the fit.

- 
- [1] C. Cercignani and G. M. Kremer, The relativistic Boltzmann equation: theory and applications (Birkhäuser Verlag, Basel, Switzerland, 2002).
  - [2] C. Marle, Annales de l'I.H.P. Physique théorique **10**, 67–126 (1969) .
  - [3] J. L. Anderson and H. R. Witting, Physica **74**, 466–488 (1974).
  - [4] J. L. Anderson and H. R. Witting, Physica **74**, 489–495 (1974).
  - [5] J. D. Bjorken, Phys. Rev. D **27**, 140–151 (1983).
  - [6] W. Florkowski, R. Ryblewski, and M. Strickland, Phys. Rev. C **88**, 024903 (2013).
  - [7] W. Florkowski, R. Ryblewski, and M. Strickland, Nucl. Phys. A **916**, 249–259 (2013).
  - [8] W. Florkowski, E. Maksymiuk, R. Ryblewski, and M. Strickland, Phys. Rev. C **89**, 054908 (2014).
  - [9] W. Israel and J. M. Stewart, Ann. Phys. **118**, 341–372 (1979).
  - [10] W. Florkowski, A. Jaiswal, E. Maksymiuk, R. Ryblewski, and M. Strickland, Phys. Rev. C **91**, 054907 (2015).

- [11] R. Ryblewski, J. Phys.: Conf. Ser. **612**, 012058 (2015).
- [12] G. S. Denicol, S. Jeon, and C. Gale, Phys. Rev. C **90**, 024912 (2014).
- [13] R. S. Bhalerao, A. Jaiswal, S. Pal, and V. Sreekanth, Phys. Rev. C **89**, 054903 (2014).
- [14] M. Mendoza, B. M. Boghosian, H. J. Herrmann, and S. Succi, Phys. Rev. Lett. **105**, 014502 (2010).
- [15] P. Romatschke, M. Mendoza, and S. Succi, Phys. Rev. C **84**, 034903 (2011).
- [16] D. Hupp, M. Mendoza, I. Bouras, S. Succi, and H. J. Herrmann, Phys. Rev. D **84**, 125015 (2011).
- [17] F. Mohseni, M. Mendoza, S. Succi, and H. J. Herrmann, Phys. Rev. D **87**, 083003 (2013).
- [18] M. Mendoza, I. Karlin, S. Succi, and H. J. Herrmann, Phys. Rev. D **87**, 065027 (2013).
- [19] R. Blaga and V. E. Ambruş, arXiv:1612.01287 [physics.flu-dyn].
- [20] R. Blaga and V. E. Ambruş, AIP Conf. Proc. **1796**, 020010 (2017).
- [21] A. Gabbana, M. Mendoza, S. Succi, and R. Tripiccione, Phys. Rev. E **95**, 053304 (2017).
- [22] A. Gabbana, M. Mendoza, S. Succi, and R. Tripiccione, arXiv:1704.02523v1 [physics.comp-ph].
- [23] R. C. V. Coelho, M. Mendoza, M. M. Doria, and H. J. Herrmann, arXiv:1706.00801 [cond-mat.soft].
- [24] I. Bouras, E. Molnár, H. Niemi, Z. Xu, A. El, O. Fochler, C. Greiner, and D. H. Rischke, Phys. Rev. Lett. **103**, 032301 (2009).
- [25] I. Bouras, E. Molnár, H. Niemi, Z. Xu, A. El, O. Fochler, C. Greiner, and D.H. Rischke, Nucl. Phys. A **830**, 741c–744c (2009).
- [26] I. Bouras, E. Molnár, H. Niemi, Z. Xu, A. El, O. Fochler, C. Greiner, and D. H. Rischke, Phys. Rev. C **82**, 024910 (2010).
- [27] P. Romatschke, Phys. Rev. D **85**, 065012 (2012).
- [28] L. D. Landau and E. M. Lifshitz, *Fluid mechanics*, 2nd ed. (Pergamon Press, Oxford, UK, 1987).
- [29] C. Eckart, Phys. Rev. **58**, 919 (1940).
- [30] L. Rezzolla and O. Zanotti, *Relativistic hydrodynamics* (Oxford University Press, Oxford, UK, 2013).
- [31] A. Jaiswal, Phys. Rev. C **88** (2013) 021903(R).
- [32] C. Chattopadhyay, A. Jaiswal, S. Pal, and R. Ryblewski, Phys. Rev. C **91**, 024917 (2015).

- [33] A. Jaiswal, B. Friman, and K. Redlich, Phys. Lett. B **751**, 548–552 (2015).
- [34] J. A. Trangenstein, *Numerical solution of hyperbolic partial differential equations* (Cambridge University Press, New York, USA, 2007).